environmental sciences proceedings

MDPI

Proceeding Paper

Aspects of Rain Drop Size Distribution Characteristics from Measurements in Two Mid-Latitude Coastal Locations †

Merhala Thurai [1,*], Viswanathan Bringi [1], David Wolff [2], Charanjit Pabla [2,3], Gyuwon Lee [4] and Wonbae Bang [4]

[1] Department of Electrical and Computer Engineering, Colorado State University, Fort Collins, CO 80523, USA; bringi@engr.colostate.edu
[2] NASA GSFC Wallops Flight Facility, Wallops Island, VA 23337, USA; david.b.wolff@nasa.gov (D.W.); charanjit.s.pabla@nasa.gov (C.P.)
[3] Science Systems & Applications, Inc., Lanham, MD 20771, USA
[4] Department of Atmospheric Sciences, Center for Atmospheric Remote Sensing (CARE), Kyungpook National University, Daegu 37224, Republic of Korea; gyuwon@knu.ac.kr (G.L.); mpq2k@naver.com (W.B.)
* Correspondence: merhala@engr.colostate.edu
† Presented at the 6th International Electronic Conference on Atmospheric Sciences, 15–30 October 2023; Available online: https://ecas2023.sciforum.net/.

Abstract: We examine several different features of DSDs based on data and observations from two mid-latitude coastal locations: (a) the Delmarva peninsula, USA, and (b) Incheon, South Korea. In each case, the full DSD spectra were obtained from two collocated disdrometers. Two events from location (a) and one event from location (b) are presented. For (a), observations and retrievals from NASA's S-band polarimetric radar are included in the analyses as well as retrieved DSD parameters from the dual-wavelength precipitation radar onboard the Global Precipitation Measurement satellite. For (b), the disdrometer-based DSD data are compared with measurements from another sensor. Our main aim is to examine the underlying shape of the DSDs and their representation by the generalized gamma model.

Keywords: rain drop size distributions; generalized gamma model; underlying shapes

Citation: Thurai, M.; Bringi, V.; Wolff, D.; Pabla, C.; Lee, G.; Bang, W. Aspects of Rain Drop Size Distribution Characteristics from Measurements in Two Mid-Latitude Coastal Locations. *Environ. Sci. Proc.* **2023**, *27*, 14. https://doi.org/10.3390/ecas2023-15510

Academic Editor: Anthony Lupo

Published: 31 October 2023

1. Introduction

Numerous studies relating to the characterization of rain drop size distributions (DSDs) have been conducted over the past several decades. One of the oldest and the most well-known examples is the Marshall–Palmer model [1], which is based on measurements in stratiform rain in Montreal and modeled in the form of an exponential distribution. Later, Ulbrich [2] used the three-parameter gamma distribution to represent the measured DSDs over shorter time scales, such as a few minutes. Since then, the gamma distribution has been extensively used by a countless number of researchers to model DSD measurements (e.g., [3–5]). Data include measurements from various types of disdrometers, such as the Joss–Waldvogel disdrometer [6], Parsivel [7], the 2D video disdrometer [8,9], and the optical disdrometer ODM470 [10,11], as well as those retrieved from dual-polarization radars [12,13] and dual-frequency weather radars [14,15]. There are also other distributions such as log-normal and Weibull distributions for representation of DSDs, but often they are used for evaluation of radiowave propagation effects on microwave and millimeter wave communication links [16].

More recently, the generalized gamma (G-G) model was introduced [17,18] for DSD analyses. It was shown that the other models used for DSDs were subsets or limiting cases of the G-G model. In a very recent review paper [19], the history of the DSD representation was presented especially using functional forms ranging from exponential and gamma models to generalized gamma models and their normalization, for example, un-normalized, single- and double-moment scaling normalized versions.

The G-G model can be formulated in terms of two reference moments [M_i, Mj] and an underlying shape function, h(x). Details of the formulation can be seen in [18]. Variability in h(x) was also examined [20]; they showed that it is sufficiently invariant, depending on the reference moments, for stratiform rain. A large database of DSD measurements from several different locations was used. Thurai et al. [21] extended this further using datasets from two different locations. They used [M_3, M_6] as well as [M_3, M_4] as reference moments. For both cases, h(x) was found to be relatively stable but with a significant spread.

In this paper, we examine three further events from two mid-latitude coastal locations in two different continents, namely, (i) the Delmarva peninsula, USA, and (ii) Incheon, South Korea. In each case, 3 min disdrometer measurements were used for the analyses. Two events from the first location and one event from the second location are presented. Though the main aim is to examine the underlying shape of the DSDs and their representation by the generalized gamma model, we also consider a few other aspects of the DSD measurements.

Figure 1 shows the two locations, marked as WFF (Delmarva) in blue and ICN (Incheon) in red. The other two locations referred to earlier are also shown: Greeley, Colorado (GXY in green), and Huntsville, Alabama (HSV in purple). They have also had similar long-term measurement programs; data from these two locations have been analyzed previously [22].

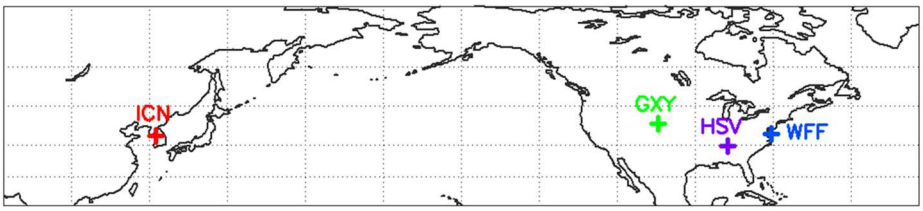

Figure 1. Locations of the two mid-latitude coastal locations: WFF in blue denotes the location at the Delmarva peninsula and ICN in red denotes the location at Incheon. The green and the purple points represent Greeley, Colorado, and Huntsville, Alabama, respectively.

2. Instrumentations and Data

2.1. Delmarva Peninsula

The instrumentation site at Delmarva peninsula contains many types of disdrometers and other rainfall measurement equipment. It is one of the ground validation 'super sites' for rainfall measurements from the Global Precipitation Measurement (GPM) satellite [23]. Amongst the instruments are (i) a Meteorological Particle Spectrometer (MPS) [24] and a 2D video disdrometer (2DVD), both installed within a second/third scaled version of the DFIR double wind fence [25]. Whilst the MPS provides accurate measurements of drop concentrations of small and tiny drops, especially below 1 mm, the 2DVD was found to be better suited for larger sized, i.e., $\geq$1 mm, drop diameters. By combining the two sets of measurements, it was possible to construct the 'full' DSD spectra. Several studies have been conducted using such datasets from this location [26,27]. The studies include DSD-based separation of stratiform and convective rain as well as light rain. An S-band polarimetric radar (NPOL) [28], situated 37 km away from the instrument site, was used for confirming the separation technique.

2.2. Incheon

In June 2021, the instruments for observing surface precipitation and cloud/precipitation systems from Kyungpook National University (KNU) were intensively installed at the Incheon weather observatory (ICO). The installed instrument from KNU includes various types of distrometers such as 2DVD, POSS [29,30], and PARSIVEL2 as well as an X-band vertically pointing radar (VertiX) [31] and a K-band vertically pointing radar (MRR-pro) [32]. In addition, a weighing rain gauge (Pluvio 200 with Belfort double alter shield) [33], 10 tipping bucket rain gauges with 0.2 mm resolution (RG3-M), and an instrument with 0.1 second resolution for observing surface wind (USA-1) were installed. As of June 2022,

the MPS (the same optical disdrometer mentioned earlier) has also been installed for observing more detailed drop size distributions. As with the Delmarva datasets, the full DSD spectra were constructed from 3 min DSDs from the MPS and the collocated 2DVD.

3. Delmarva Events

Two light stratiform rain examples from a very active 2020 Atlantic hurricane season are presented. Both had coverage from the Global Precipitation Measurement (GPM) Core Observatory satellite [34] that traversed over the Delmarva peninsula. The two events were included in a previous study [35] relating ground validation of GPM satellite observations.

3.1. Event 1

For the first of these events, which occurred on 24 September 2020, the disdrometer site captured light rain from the remnants of tropical storm Beta with borderline coverage from GPM satellite radars. Figure 2a shows the values of the mass-weighted mean diameter (D_m) estimated from the dual-frequency precipitation radar (DPR). The straight lines represent the DPR swath across the Delmarva peninsula. The red dot marks the disdrometer site and the black cross shows the location of the NPOL radar, with the dotted circles representing 50, 100, and 150 km coverage. At the disdrometer site, D_m values are around 1 mm. The 1 km by 1 km gridded reflectivity data (dBZ) from the NPOL radar are shown in panel (b). Reflectivity values are generally low, and less than 25 dBZ around the disdrometer site. Panel (c) shows the histogram of D_m values derived from the NPOL gridded data using the equation used previously for light rain [36]. Finally, panel (d) shows the variation in N_W (the normalized intercept parameter) versus D_m derived from the DPR measurements (in orange) during the satellite overpass. The green arrow shows the range of values from NPOL. They show values less than 1.3 mm and are consistent with the DPR-based D_ms. Also included in panel (d) are the N_W versus D_m variations derived from 3 min DSDs (from MPS and 2DVD) and our stratiform-convective rain partition line [27] shown as a dashed black line. In both cases, stratiform rain is indicated for the whole event.

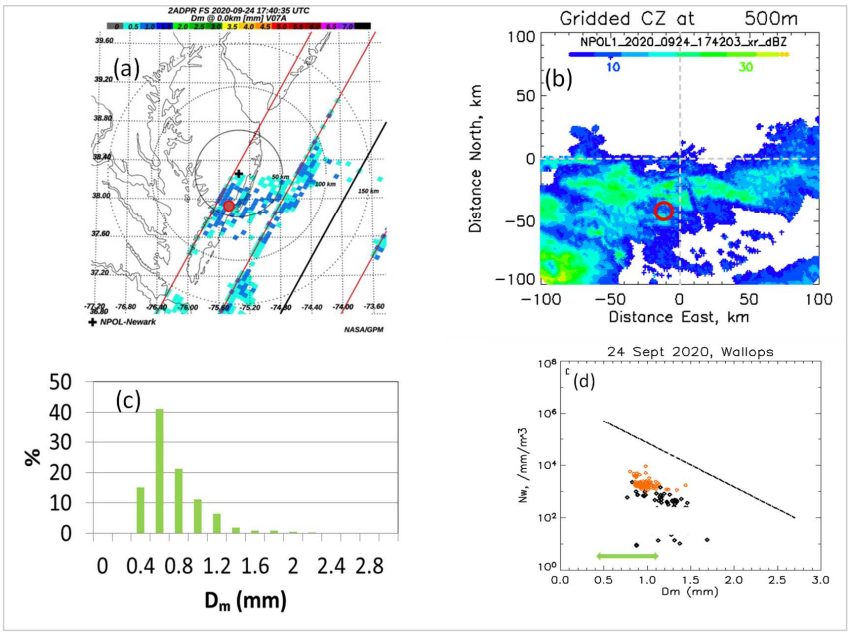

Figure 2. (**a**) The GPM DPR swath across the Delmarva peninsula during the 24 September 2020 event showing the estimated D_m (mm) values; (**b**) 1 km by 1 km gridded dBZ data from the NPOL radar during the DPR overpass; (**c**) histogram of D_m estimated from NPOL; (**d**) N_W versus D_m from DPR (orange) and from 3 min DSDs (black). The red dots in panels (**a**,**b**) show the location of the disdrometers. The green arrow in panel (**d**) shows the range of Dm values from NPOL (from panel (**c**)).

3.2. Event 2

The second event, the remnants of tropical storm Zeta, was well sampled from the ground and from space on 29 October 2020. The NPOL quasi-vertical profiles (QVPs) [37] indicate warm air advection with the approach of Zeta during the 17–19 UTC period. This can be seen in Figure 3; the four panels represent the reflectivity, the differential reflectivity, the co-polar correlation coefficient, and the differential phase, as denoted in the figure caption.

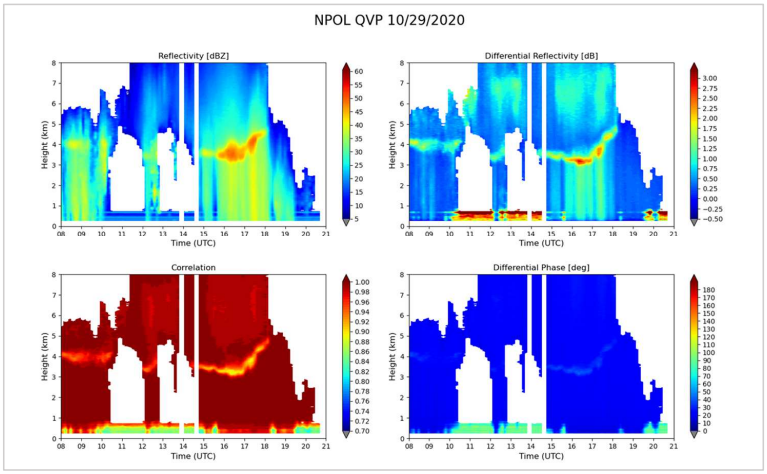

Figure 3. QVPs from NPOL indicating warm air advection with the approach of tropical storm Zeta on 29 October 2020. **Top left**: Reflectivity; **Top right**: differential reflectivity; **Bottom left**: copolar correlation coefficient; **Bottom right**: differential phase.

The GPM overpass took place earlier at 07:37 UTC, and in Figure 4a, we show the estimated D_m values from the GPM-DPR measurements. They are also low but in general somewhat higher than the first event in Figure 2a. The N_W versus D_m variations from the DPR are shown as orange points in Figure 4b. Note that some filtering has been applied by taking into account the second digit of the 'typePrecip' flag from the DPR product list. Specifically, all pixels with values of 8 or 9 have been omitted. The 3 min DSD-based N_W versus D_m is also shown (black points) together with the stratiform-convective separation line (dashed black line). Once again, in both cases, stratiform rain is indicated, though a few points lie close to the separation line.

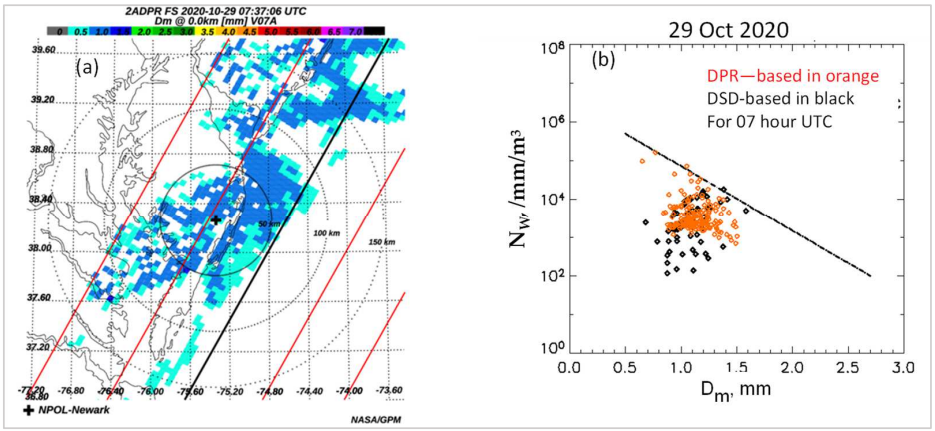

Figure 4. (**a**) The GPM DPR swath across the Delmarva peninsula during the 10 October 2020 event showing the estimated D_m (mm) values; (**b**) N_W versus D_m from DPR (range) and from 3-min DSDs (black).

4. Incheon Event

The event analyzed was a stratiform rain event with relatively thick bright band which occurred on 12 July 2022 commencing at 18:00 UTC. Observations from MRR-PRO located at the same site as MPS, 2DVD, and POSS are shown in Figure 5. Panel (a) shows the reflectivity–height profile, panel (b) shows the corresponding Doppler mean velocity, and panel (c) shows the spectral width. The melting layer at around 5 km is visible in all three panels for the entire 6 h (i.e., from 18:00 to 24:00 UTC). Shown in panels (d) and (e) are the height profiles of reflectivity and Doppler velocity, respectively, from the VertiX radar at 22 h UTC. The melting layer is clearer, both from the enhanced reflectivity around 5 km as well as the sharp increase in the Doppler mean velocity from the snow region down to the rain region.

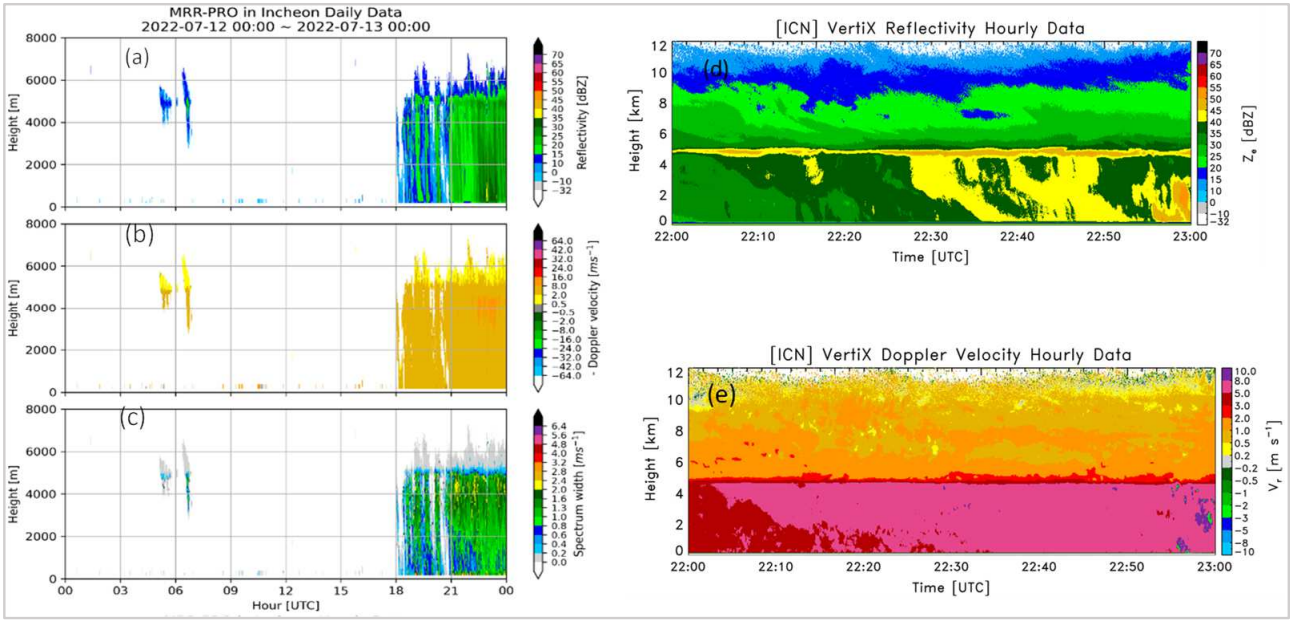

Figure 5. Observations of height profiles from MRR-PRO for the 12 July 2022 event: (**a**) dBZ; (**b**) Doppler mean; (**c**) spectrum width. Observations of height profiles from VertiX for the same event but shown only for 22 h UTC: (**d**) X-band dBZ, and (**e**) Doppler mean velocity.

The 3 min DSD spectra from 2200 to 2300 h UTC were constructed from the MPS and the collocated 2DVD measurements. They were compared with data from a precipitation occurrence sensor system (POSS), also collocated. Figure 6 shows the comparisons from 2200 to 2300 h UTC. Overall, good agreement is obtained, attesting to the high data quality of the three disdrometers, each with very different designs. Note also that the POSS has a much larger sampling volume that the other two disdrometers.

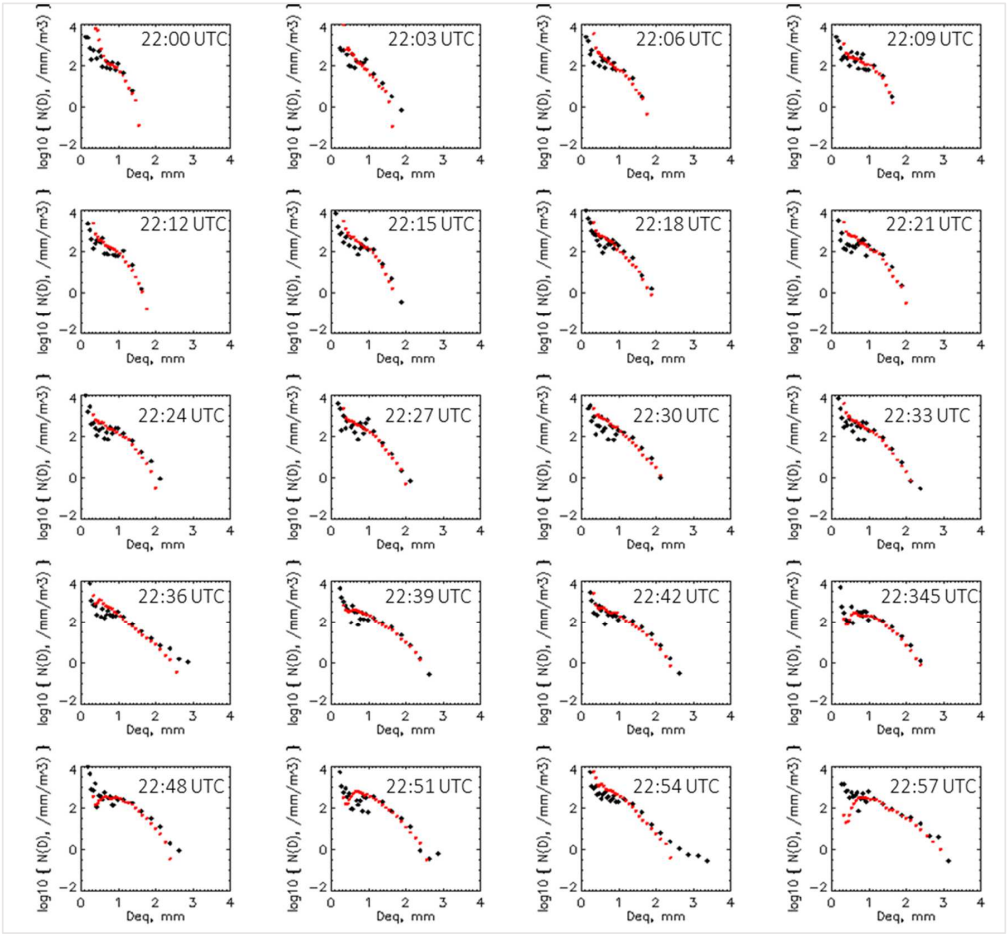

Figure 6. Comparisons of 3 min DSDs from MPS-2DVD composite data (in black) and from the POSS (in red) on the 12 July 2022, 22 h UTC.

5. DSD Analyses

Our earlier studies using datasets from Greeley, Colorado, and Huntsville, Alabama, showed that overall, the generalized gamma (G-G) model seems to capture the main features of the measured DSD shapes throughout the whole spectra [22]. The suitability of the G-G model was established for two pairs of reference moments, namely the third and fourth moments and the third and sixth moments.

In the three events considered here, the same was found to be the case. As an illustrative example, we show in Figure 7 three-minute DSD data from the Incheon event. The MPS data are shown in black (used for D < 1 mm) and 2DVD data shown in blue (used for ≥1 mm). The red curves show the fitted G-G model. Excellent representation can be seen.

On the other hand, it is equally important to examine whether the measured DSDs have a similar underlying shape, often denoted by h(x), which is related to the DSD, N(D), by the following:

$$h(x) = \frac{N(D)}{N_0'} \tag{1}$$

where

$$N_0' = M_i^{\left(\frac{j+1}{j-1}\right)} \; M_j^{\left(\frac{i+1}{i-j}\right)} \tag{2}$$

$$x = \frac{D}{D_m'} \tag{3}$$

and

$$D'_m = \left(\frac{M_j}{M_i}\right)^{\frac{1}{(j-i)}} \quad (4)$$

The nth moment, M_n, of the DSD is given by:

$$M_n = \int_0^{D_{max}} D^n N(D)\, dD \quad (5)$$

Here, D_{max} is the maximum diameter.

To derive h(x) for a given (e.g., 3 min) DSD, the following step-by-step approach can be used:

i. For a given DSD, N(D) (say over 3 min), evaluate Equation (5) to derive the values of the two selected pair of moments (these could be, for example, the third and sixth or third and fourth).
ii. Use Equation (4) to derive D_m'.
iii. For a given diameter, D, derive x (which is the 'scaled' diameter).
iv. Use Equation (2) to derive N_0'.
v. For a specific D, use N(D) and N_0' from step (iv) to derive h(x).
vi. Repeat for all diameters for a given N(D). This will provide one plot of h(x) versus x.

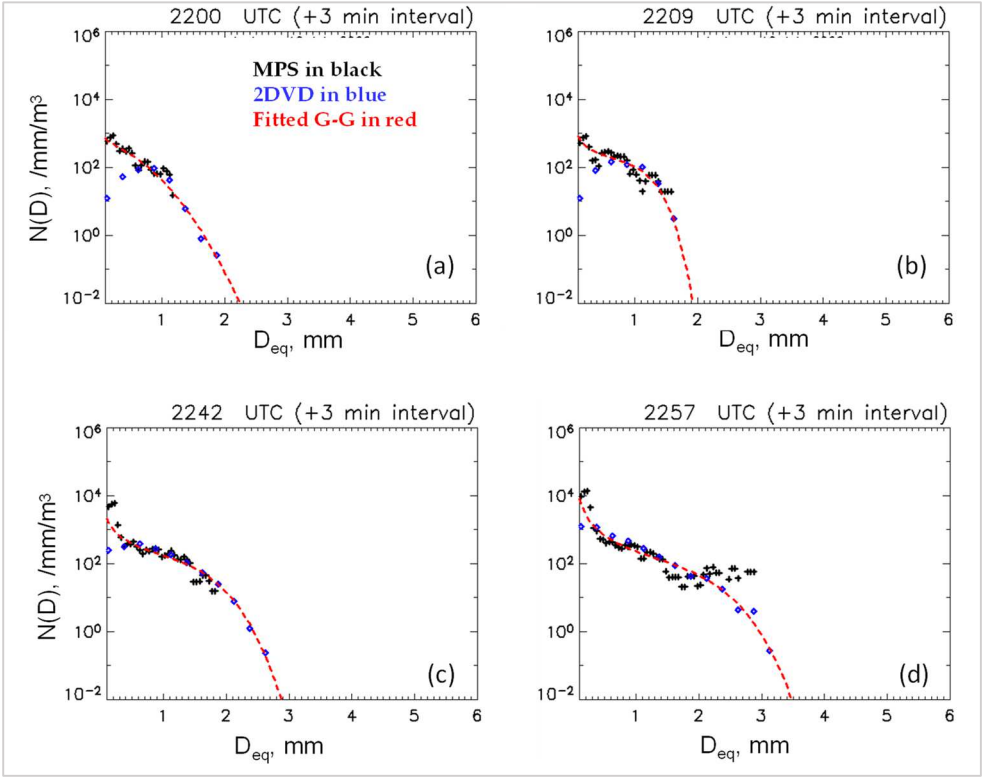

Figure 7. Four examples of 3-min measured DSDs (MPS in black and 2DVD in red) and their fitted G-G model curves for the 12 July 2022 event at Incheon. The start times are (**a**) 22:00; (**b**) 22:09; (**c**) 22:42; and (**d**) 22:57 UTC.

The process is repeated for all selected DSDs, and the underlying shape is obtained using h(x) versus x. Panel (a) of Figure 8a,b shows these plots for the two events at the Delmarva peninsula. The panel also includes the h(x) median curve derived from the fitted G-G model for more than 3000 3 min DSDs. The most probable [μ_{GG}, c] pair from the fitted

model was used to generate the black dashed curve (see Figure 7a in Reference [22]). What is noticeable is that whilst the light rain event on 24 September 2020 (17 h UTC) shows similarity with the black curve, the event on 29 October 2020 (07 UTC) shows deviation. In particular, the 'shoulder' region around x = 1 appears significantly more pronounced. Similar deviation (though not as pronounced) was found for the Incheon event on 12 July 2022 (22 h UTC), as shown in panel (b) of Figure 8. This could possibly indicate certain types of drop break-up in the large drop region as well as coalescence of small drops being more significant. Most of the other events, especially in Greeley and Huntsville, did not seem to exhibit this behavior.

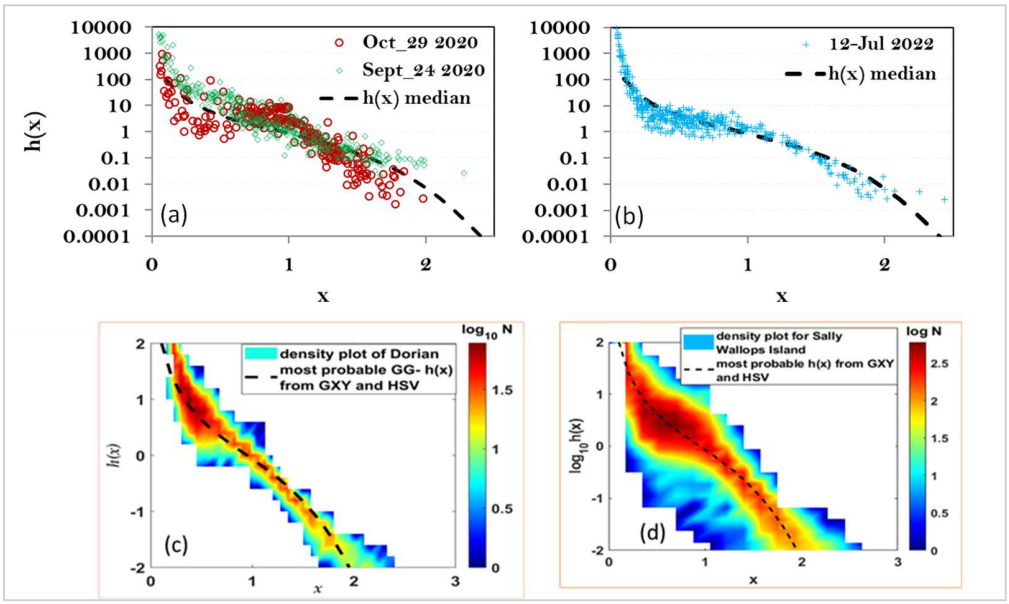

Figure 8. h(x) plots (**a**) for the two events in the Delmarva peninsula using 3 min DSDs; (**b**) same as (**a**) but for the Incheon event; (**c**) for category 1 Hurricane Dorian over Delmarva peninsula on 6 September 2019 as a color intensity plot (using 3-min DSDs); (**d**) same as (**c**) but for remnants of storm Sally on 17–18 September 2020 (using 1-min DSDs).

It is also worth noting that many of the events recorded at the Wallops site had DSDs whose h(x) were in close agreement with our most probable (or 'median') h(x) from the Greeley and Huntsville datasets. Two examples are shown in panels (c) and (d), one during category 1 hurricane Dorian (details of the analyses can be found in [26]), and the other was when remnants of storm Sally traversed the Wallops site. Both show the black curve passing through the maximum intensity of the color scale plots. For the latter, however, 1 min DSDs were used, thus showing much thicker variation (i.e., a larger spread) as one would expect when the integration time is reduced.

6. Concluding Remarks

Out of the three events presented here, two showed noticeable deviations from the most probable (or median) underlying shape, h(x), of the drop size distribution. They were both stratiform rain events and they were both in coastal, mid-latitude locations (and peninsulas). The third event, which one could categorize as a 'light rain' event, showed close agreement with our median h(x).

Other points to note from our results are as follows:

- For the light rain event at the Delmarva peninsula, NPOL-radar-based D_m values were mostly in the range of 0.4 to 1.2 mm.
- This was consistent with the GPM-DPR-based D_m estimates.
- Both the DSD-based N_W and the D_m and from GPM-DPR were below the stratiform-convective separation line.

- The second event from the Delmarva peninsula (remnants of tropical storm Zeta) also had N_W versus D_m from GPM-DPR as well as from DSD measurements below the separation line (except for a few points which were very close to the line).
- D_m values for this event were in the 1 to 1.5 mm range.
- The event in Incheon in the Korean peninsula had D_m values in the range of 0.9 to 1.6 mm, similar to the second event from the Delmarva peninsula.
- The 3 min DSDs from the MPS and 2DVD combined spectra showed good agreement with POSS-based 3 min DSDs.
- Although the generalized gamma model seems to capture the main features of the DSD shapes, the underlying shape for the two events which showed deviations in terms of h(x) had different fitted shape parameters from the most probable [μ_{GG}, c] pair.

Regarding N_W versus D_m, one would expect some form of inherent/intrinsic correlation because they are both dependent on the third and the fourth moments. Nevertheless, as has been alluded to in some earlier studies (e.g., [3,4,27,38]), where the points lie in the N_W versus D_m domain as well as the 'trend' in the variation may well depend on rain type.

We plan to compare h(x) between stratiform rain events and convective rain events (both deep and shallow), as well as light rain events from both locations. MPS, 2DVD, and POSS datasets will be utilized. It should also be noted that for the Incheon event considered here, the MPS and 2DVD were not installed inside a wind fence. For the 2023 summer observations, both instruments will be moved to another nearby site and installed within a full-scale DFIR.

Comparisons between Incheon and Delmarva datasets will also provide useful insights into similarities (or dissimilarities) since they are both in coastal mid-latitude locations located in peninsulas on two different continents (both peninsulas being on the east side of the continents).

Author Contributions: Conceptualization, M.T. and V.B.; methodology, M.T. and V.B.; formal analysis, M.T.; investigation, M.T., V.B., D.W., G.L. and W.B.; resources, D.W.; data curation, C.P., G.L. and W.B.; writing—original draft preparation, M.T., C.P., W.B. and V.B.; writing—review and editing, V.B. and D.W.; supervision, V.B., G.L. and D.W.; project administration, V.B. and D.W. All authors have read and agreed to the published version of the manuscript.

Funding: M.T. was funded by NASA's Precipitation Measurement Mission via grant award number 80NSSC19K0676. V.B. was funded by NASA's Atmospheric Dynamics program via grant award number 80NSSC20K0893 as well as the National Science Foundation, grant number AGS-1901585 to Colorado State University.

Data Availability Statement: Data can be made available upon request to any of the authors.

Acknowledgments: We would like to thank Jason Pippitt (GSFC/SSAI) for processing and QC of NPOL data, Carl Schirtzinger (ASRC/WFF) and Michael Watson (ASRC/WFF) for NPOL engineering support. We also wish to thank the many students of G. Lee at Kyungpook National University in Daegu, RoK, for their help and support in the MPS installation in Incheon and data quality assessment.

Conflicts of Interest: The authors declare no conflicts of interest. The funders had no role in the design of this study; in the collection, analyses, or interpretation of its data; in the writing of this manuscript; or in the decision to publish these results. Author Charanjit Pabla was employed by the company Science Systems & Applications, Inc. Lanham, MD, USA. The remaining authors declare that the research was conducted in the absence of any commercial or financial relationships that could be construed as a potential conflict of interest.

References

1. Marshall, J.S.; Palmer, W.M. The distribution of raindrops with size. *J. Meteorol.* **1948**, *5*, 165–166. [CrossRef]
2. Ulbrich, C.W. Natural variation in the analytical form of the raindrop size distribution. *J. Clim. Appl. Meteorol.* **1983**, *22*, 1764–1775. [CrossRef]
3. Bringi, V.N.; Chandrasekar, V.; Hubbert, J.; Gorgucci, E.; Randeu, W.L.; Schoenhuber, M. Raindrop Size Distribution in Different Climatic Regimes from Disdrometer and Dual-Polarized Radar Analysis. *J. Atmos. Sci.* **2003**, *60*, 354–365. [CrossRef]

4. Dolan, B.; Fuchs, B.; Rutledge, S.A.; Barnes, E.A.; Thompson, E.J. Primary Modes of Global Drop Size Distributions. *J. Atmos. Sci.* **2018**, *75*, 1453–1476. [CrossRef]
5. Williams, C.R.; Bringi, V.N.; Carey, L.D.; Chandrasekar, V.; Gatlin, P.N.; Haddad, Z.S.; Meneghini, R.; Joseph Munchak, S.; Nesbitt, S.W.; Petersen, W.A.; et al. Describing the Shape of Raindrop Size Distributions Using Uncorrelated Raindrop Mass Spectrum Parameters. *J. Appl. Meteorol. Climatol.* **2014**, *53*, 1282–1296. [CrossRef]
6. Joss, J.; Waldvogel, A. Raindrop Size Distribution and Sampling Size Errors. *J. Atmos. Sci.* **1969**, *26*, 566–569. [CrossRef]
7. Tokay, A.; Wolff, D.B.; Petersen, W.A. Evaluation of the New Version of the Laser-Optical Disdrometer, OTT Parsivel2. *J. Atmos. Oceanic Technol.* **2014**, *31*, 1276–1288. [CrossRef]
8. Schönhuber, M.; Lammer, G.; Randeu, W.L. One decade of imaging precipitation measurement by 2D-video-distrometer. *Adv. Geosci.* **2007**, *10*, 85–90. [CrossRef]
9. Schönhuber, M.; Lammer, G.; Randeu, W.L. The 2D-Video-Distrometer. In *Precipitation: Advances in Measurement, Estimation and Prediction*; Michaelides, S., Ed.; Springer: Berlin/Heidelberg, Germany, 2008; pp. 3–31. ISBN 978-3-540-77654-3.
10. Klepp, C.; Michel, S.; Protat, A.; Burdanowitz, J.; Albern, N.; Kähnert, M.; Dahl, A.; Louf, V.; Bakan, S.; Buehler, S.A. OceanRAIN, a new in-situ shipboard global ocean surface-reference dataset of all water cycle components. *Sci. Data* **2018**, *5*, 180122. [CrossRef]
11. Duncan, D.I.; Eriksson, P.; Pfreundschuh, S.; Klepp, C.; Jones, D.C. On the distinctiveness of observed oceanic raindrop distributions. *Atmos. Chem. Phys.* **2019**, *19*, 6969–6984. [CrossRef]
12. Ryzhkov, A.; Zhang, P.; Bukovčić, P.; Zhang, J.; Cocks, S. Polarimetric Radar Quantitative Precipitation Estimation. *Remote Sens.* **2022**, *14*, 1695. [CrossRef]
13. Kumjian, M.R.; Prat, O.P.; Reimel, K.J.; van Lier-Walqui, M.; Morrison, H.C. Dual-Polarization Radar Fingerprints of Precipitation Physics: A Review. *Remote Sens.* **2022**, *14*, 3706. [CrossRef]
14. Liao, L.; Meneghini, R. GPM DPR Retrievals: Algorithm, Evaluation, and Validation. *Remote Sens.* **2022**, *14*, 843. [CrossRef]
15. Tokay, A.; D'Adderio, L.P.; Wolff, D.B.; Petersen, W.A. Development and Evaluation of the Raindrop Size Distribution Parameters for the NASA Global Precipitation Measurement Mission Ground Validation Program. *J. Atmos. Oceanic Technol.* **2020**, *37*, 115–128. [CrossRef]
16. Sekine, M.; Chen, C.-D.; Musha, T. Rain attenuation from log-normal and Weibull raindrop-size distributions. *IEEE Trans. Antennas Propag.* **1987**, *35*, 358–359. [CrossRef]
17. Auf der Maur, A.N. Statistical tools for drop size distribution: Moments and generalized gamma. *J. Atmos. Sci.* **2001**, *58*, 407–418. [CrossRef]
18. Lee, G.; Zawadzki, I.; Szyrmer, W.; Sempere-Torres, D.; Uijlenhoet, R. A General Approach to Double-Moment Normalization of Drop Size Distributions. *J. Appl. Meteorol.* **2004**, *43*, 264–281. [CrossRef]
19. Lee, G.; Bringi, V.; Thurai, M. The Retrieval of Drop Size Distribution Parameters Using a Dual-Polarimetric Radar. *Remote Sens.* **2023**, *15*, 1063. [CrossRef]
20. Raupach, T.H.; Berne, A. Invariance of the Double-Moment Normalized Raindrop Size Distribution through 3D Spatial Displacement in Stratiform Rain. *J. Appl. Meteorol. Climatol.* **2017**, *56*, 1663–1680. [CrossRef]
21. Thurai, M.; Bringi, V.; Adirosi, E.; Lombardo, F.; Gatlin, P.N. Variability of the Parameters of the Generalized Gamma Model of the Raindrop Size Distribution. In *Precipitation Science. Measurement, Remote Sensing, Microphysics and Modeling*, 1st ed.; Michaelides, S., Ed.; Elsevier: Amsterdam, The Netherlands, 2021; Chapter 16, Paperback, ISBN 9780128229736, eBook ISBN: 9780128229378.
22. Thurai, M.; Bringi, V.; Gatlin, P.N.; Petersen, W.A.; Wingo, M.T. Measurements and Modeling of the Full Rain Drop Size Distribution. *Atmosphere* **2019**, *10*, 39. [CrossRef]
23. Gatlin, P.N.; Petersen, W.A.; Pippitt, J.L.; Berendes, T.A.; Wolff, D.B.; Tokay, A. The GPM Validation Network and Evaluation of Satellite-Based Retrievals of the Rain Drop Size Distribution. *Atmosphere* **2020**, *11*, 1010. [CrossRef]
24. Baumgardner, D.; Kok, G.; Dawson, W.; O'Connor, D.; Newton, R. A new ground-based precipitation spectrometer: The Meteorological Particle Sensor (MPS). In Proceedings of the 11th Conference on Cloud Physics, Ogden, UT, USA, 3–7 June 2002; pp. 3–7.
25. Rasmussen, R.; Baker, B.; Kochendorfer, J.; Meyers, T.; Landolt, S.; Fischer, A.P.; Black, J.; Thériault, J.M.; Kucera, P.; Gochis, D.; et al. How Well Are We Measuring Snow: The NOAA/FAA/NCAR Winter Precipitation Test Bed. *Bull. Am. Meteorol. Soc.* **2012**, *93*, 811–829. [CrossRef]
26. Thurai, M.; Bringi, V.N.; Wolff, D.B.; Marks, D.A.; Pabla, C.S. Drop Size Distribution Measurements in Outer Rainbands of Hurricane Dorian at the NASA Wallops Precipitation-Research Facility. *Atmosphere* **2020**, *11*, 578. [CrossRef]
27. Thurai, M.; Bringi, V.; Wolff, D.; Marks, D.; Pabla, C. Testing the Drop-Size Distribution-Based Separation of Stratiform and Convective Rain Using Radar and Disdrometer Data from a Mid-Latitude Coastal Region. *Atmosphere* **2021**, *12*, 392. [CrossRef]
28. Wolff, D.B.; Marks, D.A.; Petersen, W.A. General application of the Relative Calibration Adjustment (RCA) technique for monitoring and correcting radar reflectivity calibration. *J. Atmos. Ocean. Technol.* **2015**, *32*, 496–506. [CrossRef]
29. Sheppard, B.E. Measurement of Raindrop Size Distributions Using a Small Doppler Radar. *J. Atmos. Oceanic Technol.* **1990**, *7*, 255–268. [CrossRef]
30. Sheppard, B.E.; Joe, P.I. Performance of the precipitation occurrence sensor system as a precipitation gauge. *J. Atmos. Ocean. Technol.* **2008**, *25*, 196–212. [CrossRef]
31. Lee, C.K.; Lee, G.W.; Zawadzki, I.; Kim, K. A Preliminary Analysis of Spatial Variability of Raindrop Size Distributions during Stratiform Rain Events. *J. Appl. Meteor. Climatol.* **2009**, *48*, 270–283. [CrossRef]

32. Ferrone, A.; Billault-Roux, A.-C.; Berne, A. ERUO: A spectral processing routine for the Micro Rain Radar PRO (MRR-PRO). *Atmos. Meas. Tech.* **2022**, *15*, 3569–3592. [CrossRef]
33. OTT Hydromet GmbH. Operating Instructions: OTT Pluvio2 Precipitation Gauge. *OTT Hydromet.* 2010. Available online: http://www.ott.com/en-us/products/download/operating-instructions-precipitation-gauge-ott-pluvio2/ (accessed on 10 July 2023).
34. Skofronick-Jackson, G.; Petersen, W.A.; Berg, W.; Kidd, C.; Stocker, E.F.; Kirschbaum, D.B.; Kakar, R.; Braun, S.A.; Huffman, G.J.; Iguchi, T.; et al. The Global Precipitation Measurement (GPM) Mission for science and society. *Bull. Am. Meteorol. Soc.* **2016**, *98*, 1679–1696. [CrossRef]
35. Pabla, C.S.; Wolff, D.B.; Marks, D.A.; Wingo, S.M.; Pippitt, J.L. GPM Ground Validation at NASA Wallops Precipitation Research Facility. *J. Atmos. Ocean. Technol.* **2022**, *39*, 1199–1215. [CrossRef]
36. Thurai, M.; Bringi, V.; Wolff, D.; Marks, D.; Pabla, C.; Kennedy, P. Drop Size Distribution Retrievals for Light Rain and Drizzle from S-Band Polarimetric Radars. *Environ. Sci. Proc.* **2022**, *19*, 23. [CrossRef]
37. Ryzhkov, A.; Zhang, P.; Reeves, H.; Kumjian, M.; Tschallener, T.; Trömel, S.; Simmer, C. Quasi-Vertical Profiles-A New Way to Look at Polarimetric Radar Data. *J. Atmos. Ocean. Technol.* **2016**, *33*, 551–562. [CrossRef]
38. Bringi, V.N.; Williams, C.R.; Thurai, M.; May, P.T. Using dual-polarized radar and dual-frequency profiler for dsd characterization: A case study from Darwin. Australia. *J. Atmos. Ocean. Technol.* **2009**, *26*, 2107. [CrossRef]